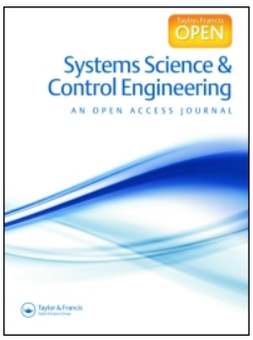

Systems Science & Control Engineering

An Open Access Journal

ISSN: (Print) 2164-2583 (Online) Journal homepage: http://www.tandfonline.com/loi/tssc20

Investigation of reductions in motor efficiency and power factor caused by stator faults when operated from an inverter drive under open loop and sensorless vector modes

M. Lane, A. Shaeboub, F. Gu & A.D. Ball

To cite this article: M. Lane, A. Shaeboub, F. Gu & A.D. Ball (2017) Investigation of reductions in motor efficiency and power factor caused by stator faults when operated from an inverter drive under open loop and sensorless vector modes, Systems Science & Control Engineering, 5:1, 361-379, DOI: 10.1080/21642583.2017.1367734

To link to this article: http://dx.doi.org/10.1080/21642583.2017.1367734

Published online: 23 Aug 2017.

SYSTEMS SCIENCE & CONTROL ENGINEERING: AN OPEN ACCESS JOURNAL, 2017
VOL. 5, 361–379
https://doi.org/10.1080/21642583.2017.1367734

Taylor & Francis
Taylor & Francis Group

Investigation of reductions in motor efficiency and power factor caused by stator faults when operated from an inverter drive under open loop and sensorless vector modes

M. Lane, A. Shaeboub, F. Gu and A.D. Ball

Centre for Efficiency and Performance Engineering, University of Huddersfield, Huddersfield, UK

ABSTRACT

The introduction of Variable Speed Drives (VSD) motor driven systems in industry is driven by the desire to increase motor efficiencies in plant. The efficiency savings are usually determined by initial energy assessments which consider factors such as the motor load type and operating conditions where the motor actual load may also be measured. However, once the system is installed and in operation, the designed-in energy efficiency of these systems may remain unchecked throughout the lifetime of the installation. Efficiency reductions may be caused by mechanical or electrical degradation of equipment that could remain undetected by the drive or user whilst the equipment appears to operate as normal. On larger systems, the financial cost of reduced efficiency can be significant. The aim of this paper is to simulate minor deteriorations in the operating conditions of a standard motor controlled from a VSD and ascertain if the worsening condition can be detected at an early stage. The deterioration in motor condition will be small enough to remain undetected by the VSD and not cause a drive fault. This paper also reviews the effect of the introduced motor imbalance on motor efficiency and introduces power factor measurement methods which can be a useful indicator of increased operating costs for equipment. Test results from the two drive operating modes of Volts/Hertz (*v*/*f*) and Sensorless Vector (SV) are compared. This is to determine if there is any noticeable difference in the measurements obtained for efficiency and power factor between drive operating modes.

ARTICLE HISTORY
Received 28 February 2017
Accepted 11 August 2017

KEYWORDS
Asymmetry; efficiency; unbalanced; stator resistance increase; motor current signature analysis (MCSA); inverter field operated controller (IFOC); random switching pattern; sensorless vector; open loop (OL); power factor; pulse width modulation (PWM)

1. Introduction

The motivation of this research is to detect early stage failure of the stator-related component of the motor. This is to be achieved by monitoring the reduction in motor operating efficiency and other parameter indicators based on power factor and time-domain based signal processing techniques. Ideally, a reduction in motor efficiency under deteriorating conditions should be able to be observed compared to the baseline efficiency at an early stage before any obvious sign of failure. It will then be possible to maintain the equipment at the efficiency level it was when first installed by early corrective intervention. There are advantages to operators of motor equipment if deteriorations in motor efficiency can be calculated on an VSD system whilst the equipment is in-service. Maintenance can then be scheduled only for when the equipment requires it. This is preferable when compared to fixed intervals which may be too frequent, resulting in unnecessary and costly intervention, or too long whereby equipment suffers catastrophic failure between inspections.

The increased use of inverter driven systems in industry can present problems for established diagnostic techniques developed solely for Direct-On-Line (DOL) AC motors. The increased noise on motor current signals caused by the VSD PWM switching frequencies can often interfere with the spectral data required for diagnostic methods using MCSA. This noise must be filtered out prior to processing of the current signals but some critical spectral data may be lost in the filtering process. Bearing related failure of motors has been extensively studied so this research has been focused on motor stator faults and efficiency reductions caused by those faults.

Studies on the total life cycle costs for motor driven systems reveal that energy costs account for 96.8% of the life cycle cost of a 1.5 kW motor and up to 99% of the costs of a 110 kW motor (Siemens Energy Efficient Drives). New motor efficiency standard IEC 60034-30-1 published in March 2014 has mandated the introduction of higher efficiency motors in a first step to reduce the energy consumption of AC motors. In the United States alone, AC motors account for 62.6% of all electricity consumed

CONTACT F. Gu F.Gu@hud.ac.uk

(Office of Energy Efficiency and Renewable Energy). Standard IEC 60034-30-1stipulates three efficiency levels for three-phase induction motors, IE1 to IE3. Phase 2 of the EU's efficiency level legislation (IE3) came into effect from 1 January 2015 stating that three-phase induction motors with a rated output from 7.5 to 375 kW must now meet the IE3 efficiency level or IE2 when operated from an inverter drive. Furthermore, an updated standard IEC 60034-30-1 now includes for IE4 motors (Efficiency classes for IEC line motors) operated DOL to the supply.

However, despite the introduction of higher efficiency motors, the use of low voltage inverter driven motor systems in industry is set to grow by a further 7% between 2016 and 2017. Presently, for every two low voltage motors sold, three low voltage drives are sold (Meza, 2014). The demand for inverter drive systems will only increase as greater energy efficiency continues to be sought.

The design of an inverter-driven motor system should be carefully considered to maximize the operating efficiency of the complete motor and inverter system. Early failure of VSD systems can be seeded before the equipment is put in service due to incorrect specification, design, installation or commissioning. A draft publication, Part 25 of standard (DD CLC/TS 60034-25:2008) aims to address these issues. It has been published to provide guidance on the design and installation of VSD driven motor systems. Annex A of the standard discusses converter types of *v*/*f* and SV. Cautionary notes are given for drive settings such as excess voltage boost values in *v*/*f* mode which can cause the motor to saturate resulting in excess heating and increased energy consumption. Electromechanical stresses and energy losses of the whole VSD driven motor system can be mitigated if the guidance in this standard is followed. This in turn will lower the risk of premature failure of the system over the expected operational lifespan.

The standard also details some of the parameters that can have a notable effect on system efficiency. Figure 1

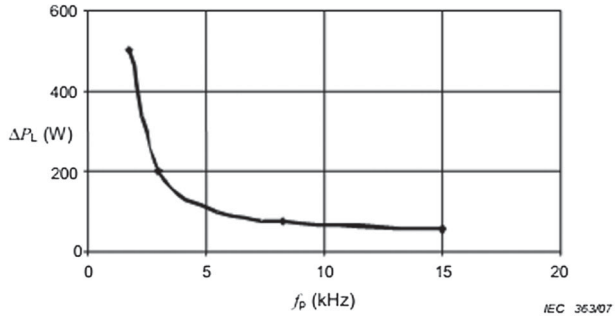

Figure 1. Losses of motor ΔP_L due to switching frequency f_P (DD CLC/TS 60034-25:2008).

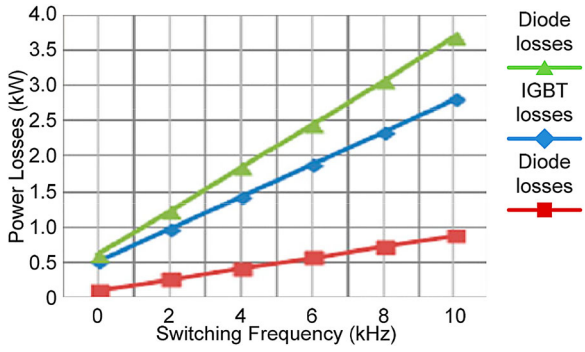

Figure 2. Losses of an inverter ΔP_L due to switching frequency f_P (Rao & Chamund, 2014).

taken from the standard DD CLC/TS 60034-25:2008 illustrates the effect that different inverter switching frequencies f_P can have on the power losses ΔP_L in the motor. As can be observed, a switching frequency of 2.6 kHz or less results in substantially greater power losses in the motor. This is due to the increased peak harmonic currents circulating in the motor windings caused by the reduced switching cycle.

Conversely, losses in the inverter switching device increase with a higher switching frequency f_p. Figure 2 is taken from tests conducted on a 1200A Insulated Gate Bipolar Transistor (IGBT) (Rao & Chamund, 2014) of the type used in modern VSD's. As can be observed from this figure, losses in the power module increase linearly with each increase in f_p. It is therefore important to strike the correct balance between motor and VSD losses when selecting a drive switching frequency.

The efficiency of an installation can also be reduced if the motor flux control method is incorrectly selected for the application. Two different motor operating modes are described as an example. The first is defined as fan or quadratic torque mode as defined by $T \alpha n^2$ where T is motor torque and n the operating speed. This mode is used in fan applications where there is less torque required at lower speeds. The inverter drive can be programmed to observe this law so that motor flux or magnetizing current is reduced at low speeds, thereby saving energy.

The second operating mode is constant torque mode $T =$ constant. In this case, the motor must have full torque or magnetizing current available at low speeds. Such an example might be a lift or hoist application. The inverter drive is therefore programmed to follow this constant-torque law. An inverter drive set to constant torque mode but controlling a fan application will perform the same as if it were set to the fan law mode but will consume more energy. Optimal flux control of motors fed from inverter drives has been studied by

Table 1. Motor failures by component.

Type of fault	Percentage failure
Bearing related	41
Stator related	37
Other	12
Rotor related	10

Kirschen, Novotny, and Suwanwisoot (1984). The research found that motor losses could be minimized by using an optimized excitation control method based on the actual machine parameters rather than the standard linear *v/f* mode. This work can be viewed as a precursor to the control method options of constant or fan law in modern PWM drives. Some VSD manufacturers have programmable curves for control of the motor flux.

Once the designed motor system has been commissioned and in operation, the system efficiency and reliability becomes influenced by other external factors. Statistics on AC motor failures reported by the Electric Power Research Institute EPRI report that motor percentage failures could be classified as given in Table 1.

Failure of the stator may occur due to thermal, mechanical, electrical or environmental stresses (Bonnett & Soukup, 1992). Some stator related faults are turn-to-turn faults, coil to coil fault, phase to phase fault, phase to ground fault and open circuit faults (Karmakar, Chattopadhyay, Mitra, & Sengupta., 2016). Other external influences of stator asymmetry are varied but could be attributed to the following factors:

- Wiring connection corrosion
- Atmospheric or mechanical effects in the drive or motor terminations
- Cable faults
- Poor initial installation techniques or equipment.

Should one stator phase become imbalanced due to a small initial fault, such as a turn to turn short-circuit then this will result in unequal current flows in the motor phases. This causes increased stresses and losses to occur in the motor windings. A further effect of this imbalance is torsional oscillation of the rotor due to torque pulsations caused by imbalanced current flows (Mirabbasi, Seifossadat, & Heidari, 2009). This in turn shortens the lifespan of the equipment and in severe cases can result in total mechanical failure.

The National Electrical Manufacturers Association (NEMA) publish recommended derating factors for motors. Figure 3 shows a derating factor curve. This curve should be applied to motors running from a supply voltage imbalance so that the expected service lifespan of the motor can be achieved. The Derating Factor (DF) is

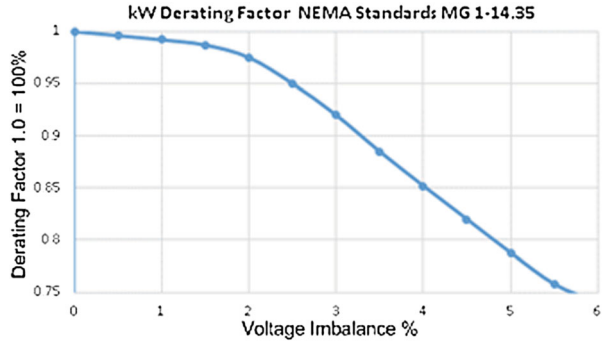

Figure 3. NEMA derating curve to apply for voltage imbalances. Diagram produced with reference to NEMA standard MG 1-14:35.

normalized so that 1.0 = 100%. A DF value of 100% indicates that the motor can be used at 100% power rating. The Voltage Imbalance (VI) axis is not scaled so a value of 1 = 1%. As an example, a 15 kW motor operating on a supply with a 4% imbalanced from phase-to-phase is considered. Reading from the derating curve, the DF for a 4% imbalance is 0.85 (or 85%). Thus, the maximum de-rated output power P_{der} that can be obtained from that motor is calculated as

$$P_{der} = P \cdot dF = 15.0 \cdot 0.85 = 12.75\,kW \quad (1)$$

where P is the power rating of the motor in kW. If this power output did not satisfy the load requirements at the expected voltage imbalances, then a higher power motor would have to be used.

McCoy and Douglass (2000) published guidance notes for industry on maintaining efficiency of plant especially when subject to voltage imbalances. It is stated that voltage imbalances of even 1% require a motor to be derated (see Figure 3). Stator resistance imbalances on an AC motor have the same effect as an imbalanced supply and if unchecked can also lead to premature motor failure. One cause of this premature failure is due to the heating effects resulting from imbalanced operation. Montsinger's rule states that an increase in motor temperature by 10°C will lead to a reduction in the motor expected operational lifespan by 50%.

Studies by Zhang, Zhao, Zhou, and Huang (2014) concerned the detection of open circuit faults in PWM converters using the motor current signals measured. This causes imbalance on the supply to the motor. Results of the test measurements are observed after transforming the *a, b, c* phase currents into *d* and *q* reference frames for analysis. The diagnostic method was proved to work for single and double transistor open-circuit faults. Investigations into any motor efficiency reductions were not carried out.

Lee et al. (2011) proposed a new strategy for condition monitoring of adjustable speed induction machine

drive systems. The strategy could be used for off-line analysis of drive system components. The drive components could be DC link capacitors, electrical cabling, stator and cable insulation, stator core and rotor bars. The off-line technique does not require spectral analysis of the motor signals or reference to the motor mathematical model. Being an off-line test, it is independent of motor operating conditions such as frequency or load that would otherwise have to be considered in an on-line system. Resistive imbalances can be measured when the motor is at standstill from the DC link voltage and this can help to benchmark motor connection conditions at stages in the motor operating life.

Salomon et al. (2015) presented work on induction motor efficiency evaluation using an air-gap torque method. The technique developed sensorless torque equations and used particle swarm optimization methods on the data obtained. This work was carried out on a VSD fed from a DOL source. The output torque estimated using the calculations was compared to the mechanical output torque and considered a good approximation.

Li, Liu, Lau, and Zhang (2015) present a novel method to determine the motor efficiency under variable speed and partial load conditions. The model was tested on a healthy motor connected to a VSD. Calculations were based on the motor speed and power taken from the VSD standard analogue or digital communication outputs. The calculation errors for this model were found to be $\pm 5\%$ for 4-pole motors under constant speed conditions. The model accuracy is more uncertain at lower speed ratio conditions.

MCSA is proven to reliably detect motor faults including winding inter-turn faults, air-gap eccentricity and broken rotor bars. Rasool and Ebrahimi (2011) combined MCSA and examination of Rotor Slot Harmonics (RSH) to diagnose inter-turn short-circuit faults in motor stator windings on non-VSD driven motors.

Akar and Gercekcioglu (2017) researched the use of Instantaneous Power Factor (IPF) signals for the diagnosis of misalignment faults in inverter-fed induction motors. Two operating speeds and five different load ranges were used for the test. At each speed and load a healthy unit was compared to six faulty states. The techniques used Fast Fourier Transforms (FFT) on the instantaneous power factor signal to study any additional harmonics generated because of the fault. It was noted from the experimental work that amplitude increases at $2f_r$ and $3f_r$ both indicated a fault from the healthy state. However, only the frequency $3f_r$ allowed the fault type and severity of fault to be determined. It found instantaneous power factor signals to be more efficacious in providing a clearer fault picture because of the combination of motor current and voltage signals.

(Drif & Marques Cardoso) researched new fault detection techniques of IPF signature analysis in detecting rotor cage faults. It was found that broken rotor bars could be detected in the sideband component at low frequencies. The techniques yielded good results for varying degrees of fault severity. A normalized severity factor based on the fault amplitude compared to the instantaneous power factor gave a good indication as to the machine condition.

Ibrahim, Badaoui, Guillet, and Bonnardot (2008) researched the use of power spectrum density techniques based on IPF for detection of bearing faults. Vibration and instantaneous speed techniques were used alongside motor stator current analysis. Torque oscillations in the stator currents were found to be predictable based on the fact a relationship exists between torque pulsations and resultant current ones. Wiener filtering techniques were carried out on the supply frequency followed by phase estimation of the phase of the signal. This processing allowed the IPF technique to provide the best indicator of faults. Spectral analysis of IPF signals were shown to highlight the defects although prior knowledge of the frequency components for the defect must be known in advance for the signal spectra to be of use.

Arabacı, Bilgin, and Ürkmez (2011) studied the use of one phase current and voltage of a squirrel cage induction machine to calculate the power factor for a healthy machine and one with a broken rotor bar. Power factor oscillations in both time and frequency domain were observed. The severity of faults could be ascertained from the frequency spectra results. In addition to the results obtained, a classification technique was developed that could detect and classify faults from the power factor. This research did not study any effects of stator imbalance on power factor or system efficiency.

Shnibha and Albarabar (2012) applied the use of only measured current for the monitoring of power factor. The work detects very low phase imbalanced faults and misalignments. The ability to use only the motor current is facilitated by using the motor nameplate data to calculate the motor reactive currents.

de Souza-Ribeiro, Jacobina, Nogueira Lima, and Cunha Oliveira (1997) studied the effects of motor parameter sensitivity on the Model Reference Adaptive Controller (MRAC) used in a VSD. The study focused on the effect that changes in stator resistance r_s had on the operation of the drive control loop for performance and speed holding. However, the research did not extend to covering motor drive system efficiency changes resulting from changes to the stator resistance.

Mouli Chandra and Tara Kalyani (2012) studied the effects that changes in motor stator resistance had on the vector control model. A model was studied that estimated

the stator resistance directly from the stator quantities. The performance of the vector controller in controlling motor torque with and without stator resistance estimation was studied. Motor transient performance and torque control was improved but no effects on motor efficiency were noted.

In this research paper, details of new work on detecting power factor and motor efficiency changes on a VSD-driven motor system with stator winding asymmetries are presented. Both SV and *v/f* VSD control modes are considered for this work. Motor voltage and current signals are analysed for a healthy motor and compared to one with simulated stator winding faults. This paper establishes that motor efficiency, voltage and current unbalances and instantaneous power factor can all be calculated from the measured signals obtained. This data can then be used as a diagnostic method for detecting imbalances.

2. Motor model

Figure 4 shows the steady state equivalent of an induction motor. r_1 and x_1 represent the stator resistance and inductance respectively. r'_2 and x'_2 are the rotor resistance and inductance. The load applied to the motor is represented by a variable resistance (Hou, Gu, Gao, Feng, & Li, 2008).

The motor speed n_0 is calculated as follows:

$$n_0 = \frac{60f}{p} \tag{2}$$

where f is the supply frequency and p the number of pole pairs. Slip, s is calculated as:

$$s = \frac{n_0 - n}{n_0} \tag{3}$$

where n is the synchronous speed of the motor.

Electrical power P_e of the system is given by Crowder (2006):

$$P_e = 3U_1 I_1 \cos\phi \tag{4}$$

where U_1 is the line voltage and I_1 the line current in the stator. Mechanical power P_m developed by the rotor is given as:

$$P_m = 3I'^2_2 r'_2 \frac{1-s}{s} \tag{5}$$

where I'_2 is the rotor current and r'_2 the rotor resistance.

From these equations, efficiency n is:

$$n = \frac{P_e}{P_m} = \frac{U_1 I_1 \cos\phi}{I'^2_2 r'_2 (1-s/s)}. \tag{6}$$

Total electrical apparent power, $P^{\wedge}$ is given as:

$$P^{\wedge} = \sqrt{3}VI \tag{7}$$

and power factor defined as

$$PF = \frac{P_e}{P^{\wedge}} = \cos\phi \tag{8}$$

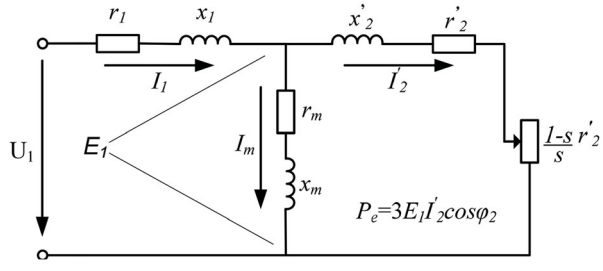

Figure 4. Induction motor equivalent circuit (Hou et al., 2008).

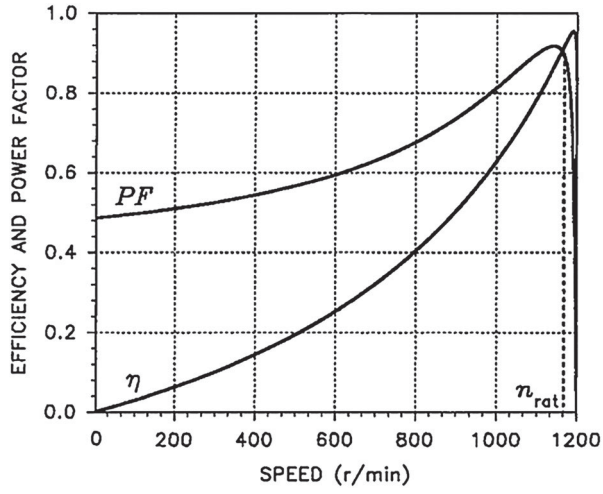

Figure 5. Efficiency and power factor versus speed for a 6-pole pair 3-phase induction motor (Trzynadlowski, 2001).

The power factor of a motor under normal running conditions depends upon the actual operating conditions in-service. A power factor and efficiency curve for a 3-phase, 22.4 kW, 6-pole AC motor with a rated speed of 1168RPM (60 Hz supply) is shown in Figure 5. As can be observed from the diagram, the normal running power factor of this motor is 0.8 at full speed. At reduced speeds the power factor can be near to 0.5. At speeds above the motor rated speed, power factor is significantly reduced. The most efficient operating region n_{rat} is at motor rated speed $n - s$ which is the synchronous speed n less slip speed s as given in Figure 5.

3. Test facilities and fault simulation

3.1. Test rig

The test rig shown in Figure 6 is designed to have a test driving AC motor and a loading DC motor. The AC motor is

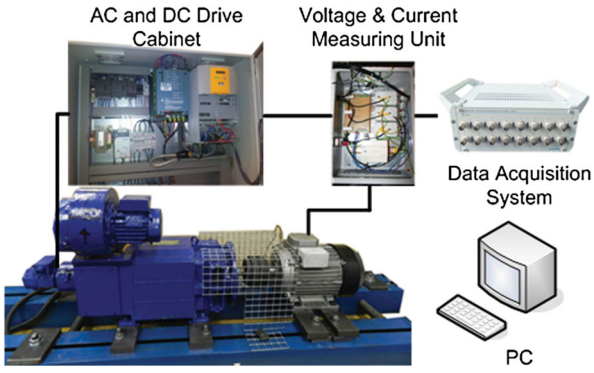

Figure 6. Laboratory test rig.

a three-phase induction motor with rated output power P_r of 4 kW at a base speed N_{rated} of 1420 RPM (two-pole pairs). Motor rated current I_{rated} is 9.2A with magnetizing current I_m of 5.2A. Instantaneous power factor of the 4 kW motor is calculated during the tests based on the phase angle difference between motor voltage and current. These results are presented in section G. The AC motor is driven by a Parker 690 PWM inverter with 3 kHz switching frequency and a carrier frequency selected by a random pattern generator enabled by default.

The DC motor is a shunt-wound design to apply different loading to the AC motor drive system. The speed, load and test duration are all programmable from a Siemens PLC thereby allowing for accurate and repeatable motor loading. The DC motor regenerates to the mains supply through a four-quadrant two phase DC drive.

Data is captured using a Sinocera 24Bit A/D Data Acquisition unit and imported into MATLAB for further processing.

3.2. Operating conditions

Two separate test cycles were applied to the rig and each test was repeated three times to ensure accuracy of the test method. Test 1 consists of a constant load with the motor run at 5 speed steps in both *v/f* and SV modes. Test 2 uses a constant speed with variable load run in SV mode only and 5 load setpoint steps used. Figure 7 illustrates the two test methods used.

The test run data detailing test run speeds, duration of test and AC motor loading is presented in Table 2.

3.3. Motor baseline data

To provide a reliable comparison between a healthy motor and one with simulated faults, two separate test runs for a healthy motor were run with the motor at normal operating temperature. The results from these test runs are referred to as the baseline test data set. Both

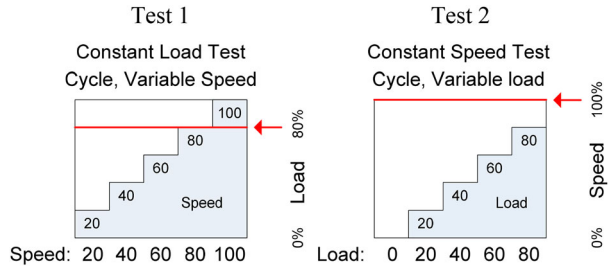

Figure 7. Test cycles and example plot.

Table 2. Test cycle data.

Test 1: Constant load, variable speed test			
Speed setpoint %	Speed RPM	Step duration(s)	Load (% of motor FLC)
20	284	120	80
40	568	120	80
60	852	120	80
80	1136	120	80
100	1420	120	80
Test 2: Constant speed variable load test			
Load setpoint (%)	Speed RPM	Step duration(s)	Speed (% of motor rated)
0	1420	120	100
20	1420	120	100
40	1420	120	100
60	1420	120	100
80	1420	120	100

Table 3. Drive operating modes.

	Drive modes
1.	Healthy motor auto-tuned – Baseline (BL)
2.	Motor with simulated stator fault of 0.4 Ω (R04)
3.	Motor with simulated stator fault of 0.8 Ω (R08)

baseline data sets were compared with each other and the results were found to be consistent between each test. This proves that the testing methods are consistent and repeatable.

3.4. Fault simulation

For comparative healthy and faulty motor data, the drive would be run for each test cycle in the following three modes as follows (Table 3):

A number of phase resistance increments are available on the test rig in 0.1 Ω steps obtained by changing the wiring tapping on the custom-built resistor unit.

The resistance fault simulated is that which occurs in phase 1 winding inside the AC motor thereby affecting only one motor phase in a star-connected motor. This is indicated in Figure 8.

The connecting cable resistance from drive to motor was measured at 0.3 Ω for each phase. Therefore, at the maximum fault resistance introduced of 0.8 Ω the total

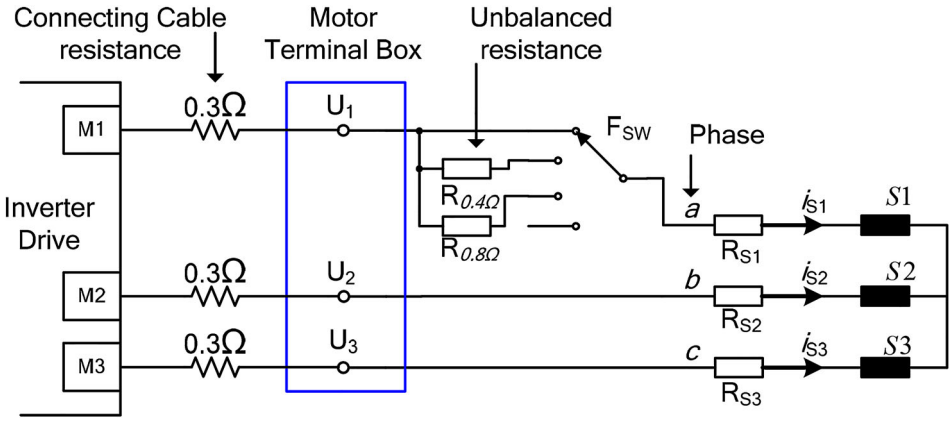

Figure 8. Motor magnetizing circuit detailing the stator phase resistance fault inserted in one of the three phase connections internally in the motor on phase 1 (STAR circuit).

resistance between the drive and motor is increased from 0.3 to 1.10 Ω in the faulty phase leg. The additional fault resistance inserted will be referred to as the resistance R_{fs}. The effect of a resistance increase in one phase of the stator equivalent circuit equation in a star connected machine is given by:

$$V_{s1} = R_s i_s + \frac{d\psi_{s1}}{dt} \rightarrow V_{s1} = (R_{fs} + R_s) i_s + \frac{d\psi_{s1}}{dt} \quad (9)$$

This imbalance created in the stator circuit has the effect of reducing the magnetic flux generated by one of the stator windings in proportion to the value of R_{fs}. The effect of this is to be studied for motor inefficiencies compared to normal running conditions.

It is proposed to use algorithms developed in MATLAB to calculate motor efficiency based on the following measurements taken from the test rig:

- Phase voltages *a, b, c*
- Phase currents *a, b, c*
- Motor speed

Motor temperature is also monitored and recorded so that the general operating conditions of the motor can be observed. This ensures that the effect of motor temperature on the measured results is kept to an absolute minimum.

3.5. VSD operation of the test rig

The inverter drive fitted to the test rig can operate in either *v/f* or SV modes. *v/f* mode is a simple method of controlling an induction motor and is widely used in low-cost drives. The *v/f* principle is that a constant ratio of motor voltage to frequency is maintained and that in turn leads to a constant motor flux φ.

$$\varphi \propto I_u \propto \frac{V}{f} \quad (10)$$

where I_u is the magnetizing current, V the output voltage and f the output frequency. Motor torque T_q produced is proportional to the vector product of the flux and motor current.

$$T = \varphi \cdot I \quad (11)$$

In order that the motor can produce as much torque as possible for a given current, the maximum amount of motor flux as possible should be maintained at all operating points. However, this can be wasteful of energy if the application does not require maximum torque at all operating points. For a fan or pump, because of low torque requirements at low speeds, magnetizing flux and current can be reduced. A linear *v/f* curve and a comparison with a parabolic curve (Siemens Sinamics S120) typically used on fan/pump installations is shown in Figure 9.

An indication of the increase in motor operating efficiency available by selecting the correct operating mode of the drive can be explained. If, for example the drive was set to run a fan using the linear law option, at 50% speed the motor magnetizing current can be reduced by up to 24%. Operating a drive in linear *v/f* mode on a fan application is wasteful of energy and may even go unnoticed in real-world applications.

On the motor test rig, the operating mode is constant torque with a linear *v/f* because it is possible to apply full load to the motor across the operating speed range of the motor.

To understand how the SV motor model in a PWM VSD can affected by a modification to stator resistance and thus affect the efficiency of the overall system, the model description of a VSD with the same operating principles as that used in the test rig has been studied. For a SV VSD to

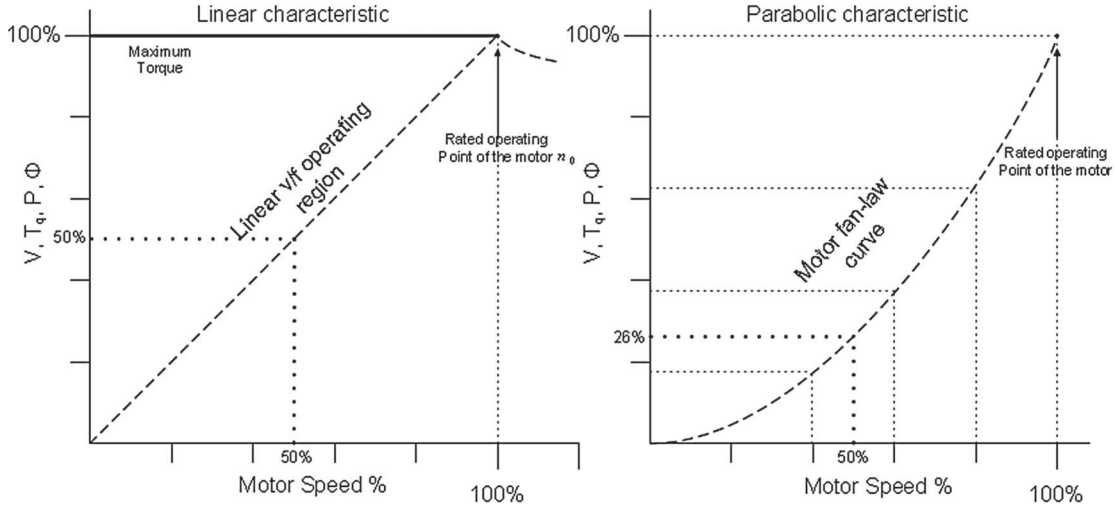

Figure 9. Operating areas and characteristic curves for an IM operating under different inverter control modes (Siemens Sinamics S120).

Table 4. Autotune parameters calculated.

Parameter	Unit
Magnetizing inductance	L_M
Leakage inductance	$L_{\sigma S}$
Rotor resistance	R_R
Stator resistance	R_S

control the motor to maximum efficiency, the drive must first be auto-tuned to match the motor to be controlled. The inverter drive used in this test rig calculates the following values for use by the VSD motor model during the autotune process (Table 4):

The model is only calculated once by the autotune function and usually when the motor is first commissioned and at normal ambient room temperature. The motor should also be de-coupled from any load to obtain correct tuning parameters. Once the auto-tune is complete and the drive is operating normally, the VSD drive in the test rig does not have an adaptive model to compensate for any changes in stator resistance during operation. Some drive manufacturers read in the exact motor temperature via a Positive Temperature Coefficient (PTC) device. This temperature is input to the drive vector control algorithm to compensate for temperature-related changes. To understand the influence of the motor model used in the test rig VSD on drive operation, a block diagram of a generic Inverter Field Oriented Controller (IFOC) inverter drive is given in Figure 10 (Zaky, 2012).

ω^*_r is the demanded speed, λ^*_{dr} the demanded rotor flux. When calculating what the current demand output should be from the IFOC current controller, feedback from the actual motor current and voltage signals are used. These are transformed from *abc* frame to *dqs* and from there the rotor angle θ_r can be estimated. The frequency and voltage output from the inverter are therefore dependent on the rotor speed, predicted by the speed estimator. However, for the speed estimator to calculate speed accurately, the motor parameters stored in the drive for the motor model must correspond to the actual motor values.

For SV operation, estimated rotor speed $\hat{\omega}_r$ is calculated from the stator current and voltages based on the

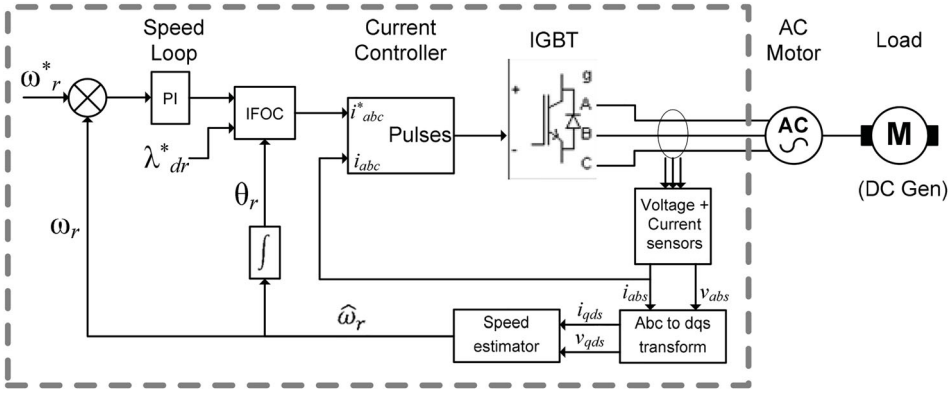

Figure 10. Inverter FOC diagram.

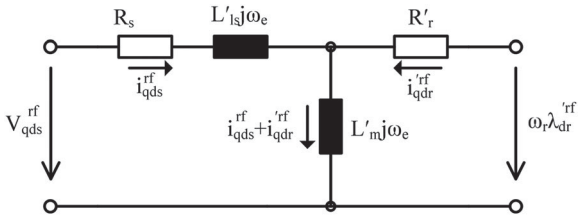

Figure 11. Induction motor steady state equivalent circuit.

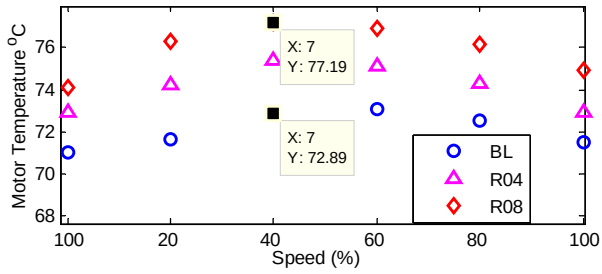

Figure 12. Motor temperature variation under each test.

steady state equivalent circuit of an induction motor shown in Figure 11 as follows:

$$\hat{\omega}_r = \frac{E}{\lambda_{dr}^{rf}} - \frac{R_r}{L_r} \cdot \frac{L_m \cdot i_{qs}^{rf}}{\lambda_{dr}^{rf}} \tag{12}$$

Where E, the air gap voltage is calculated based on the rotor stator resistance R_r and inductance L_r:

$$E = V_{qds} - R_s \cdot i_{qds} - \frac{d}{dt} \cdot L_{is} \cdot i_{qds} \tag{13}$$

If the air gap voltage value is incorrect because the stator resistance R_s stored by the motor model in the drive is in error, then the rotor speed $\hat{\omega}_r$ estimated by the drive will also be in error.

The simulated fault resistance will therefore not be compensated for by the drive controller and it is expected that motor performance will be affected by the faults introduced.

4. Stator imbalance simulation test results

This section details and compares the test results obtained from the baseline tests and compares these to the simulated fault tests for stator resistance imbalances for various speed and loading conditions. It should be noted that the motor was brought up to normal operating temperature prior to the simulated tests being commenced. This is to conform to recommendations from EN 60034-2-1:2014 that specifies standards for motor efficiency tests (BS EN 60034-2-1:2014).

4.1. Test preconditions

Following a period of prolonged running at 80% load, a stable motor operating temperature was reached. The worst-case temperature difference was recorded at 4.3°C across all tests as observed in Figure 12.

BL: Healthy Motor (Baseline data);
R04: 0.4 Ω Fault resistance introduced in phase a
R08: 0.8 Ω Fault resistance introduced in phase a

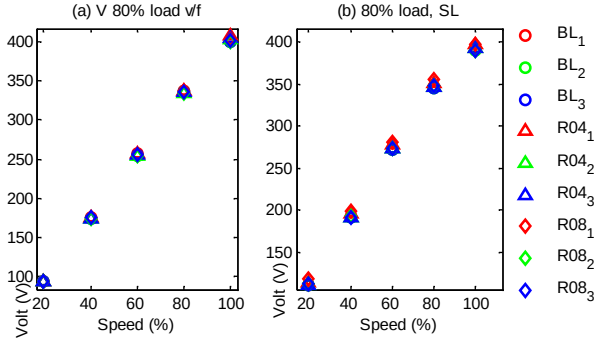

Figure 13. Plot of voltage for each phase with 80% load setpoint.

4.2. Motor terminal voltages

Figure 13 shows a plot of motor voltage taken at each speed increment with constant load setpoint of 80%. Results for a healthy motor and simulated stator imbalance conditions of 0.4 and 0.8 Ω are plotted. Tests from *v/f* (a) and SV (b) VSD modes are shown.

The subscript in BL_x denotes the motor phase number where $x = 1$ to 3. For example:

BL_1 = Baseline (Healthy Motor) phase 1;
$R04_2$ = Voltage measured in phase 2 for the stator resistance imbalance of 0.4 Ω
$R08_3$ = Voltage measured in phase 3 for the stator resistance imbalance of 0.8 Ω.

Closer examination of the plot Figure 13 is required to view the difference in stator phase voltages in sufficient detail so that a comparison can be made between healthy and simulated fault conditions. Figure 14 shows the increased detail from Figure 13 at 20% speed with 80% load. The results indicate that the baseline phases are all grouped under healthy conditions. Motor phase voltages are more dispersed under *v/f* mode (a) than SV operation (b). As the fault resistance is introduced, the phase at fault, Ph1 can be observed to separate away from the healthy phases in both cases *v/f* and SV. However, each resistance increment in SV mode (b) can be more clearly

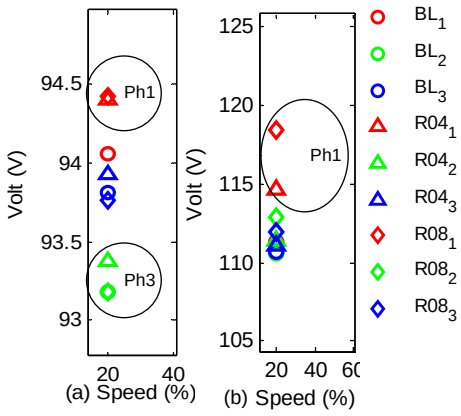

Figure 14. Plot of voltage for each phase at 100% load setting and 20% speed.

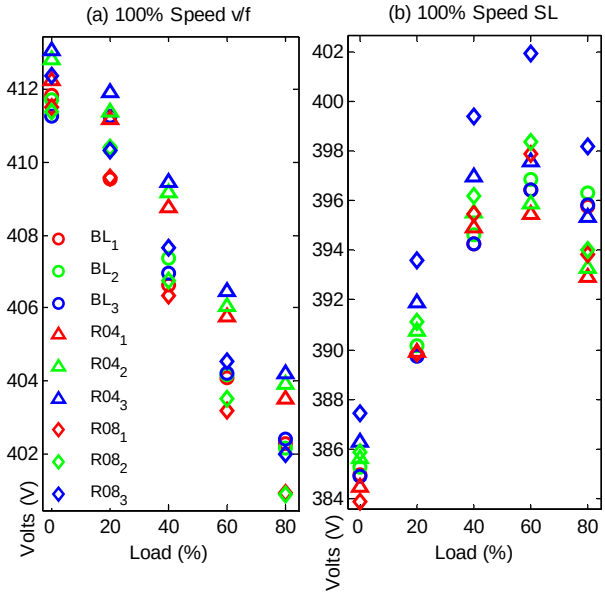

Figure 15. Plot of voltage for each phase with 100% load setting.

observed than in *v/f* mode where each resistance increment causes the same voltage increase. This is because A VSD in SV mode is constantly modifying the motor current, output frequency and phase angles to maintain a constant motor speed based on a speed observer. It follows that each motor phase voltage and current is controlled and the drive attempts to keep the phases balanced based on current feedback transducers in the drive and the SV control loop output. Because phases 2 and 3 in SV mode are more closely matched in terms of voltage under healthy and imbalanced running, this means that phase 1 will show the greatest increase under faulty conditions. In contrast, *v/f* control mode methodology is to maintain a constant *v/f* profile with no feedback and therefore no control loop feedback for motor phase currents. From the results, it is only possible to distinguish the difference in each motor phase resistance increase when operating in SV mode (b). In *v/f* mode (a) there is no clear indication whether phase 1 (Ph1) or phase 3 (Ph3) has the imbalanced resistance introduced.

BL_x: Baseline (Healthy Motor)
$R04_x$: Stator Resistance imbalance of 0.4 Ω;
$R08_x$: Stator Resistance imbalance of 0.8 Ω.
Ph1: Phase 1

Where subscript $x = 1$ to 3 for each motor phase

BL_x: Baseline (Healthy Motor)
$R04_x$: Stator Resistance imbalance of 0.4 Ω;
$R08_x$: Stator Resistance imbalance of 0.8 Ω.
Ph1: Phase 1

where subscript $x = 1$ to 3 for each motor phase.

Figure 15 displays the variable load, constant speed tests results. From this, it can be observed that the voltage of each phase is increased at lighter loads under *v/f* conditions (a) compared to SV (b). There is no distinguishable difference in test results obtained for a healthy motor compared to one with the imbalanced fault.

4.3. Motor phase currents

A plot of motor current was taken at a constant 80% load setpoint with variable speed and the results are shown in Figure 16. The current plot indicates that current in phase 1 is reduced for the 0.4 and 0.8 Ω resistance increases in both *v/f* (a) and SV modes (b). It can be observed that the healthy motor phases are closely grouped for SV mode whereas they are more dispersed in *v/f* mode. The resistance imbalance is observed to affect motor phase 1 current with both 0.4 and 0.8 Ω resistances indicating a greater reduction in *v/f* mode (a) especially so at lower motor speeds compared to SV. The imbalanced fault is clearly shown in either drive mode *v/f* or SV.

BL_x: Baseline (Healthy Motor)
$R04_x$: Stator Resistance imbalance of 0.4 Ω;
$R08_x$: Stator Resistance imbalance of 0.8 Ω.
Ph1: Phase 1

where subscript $x = 1$ to 3 for each motor phase.

Figure 17 compares the motor currents for each phase under constant speed conditions with variable load. The imbalanced phase currents are easier to distinguish in *v/f* mode under variable load operating conditions and particularly at lighter motor loads compared to SV mode. However, if the 80% load setting is observed more closely

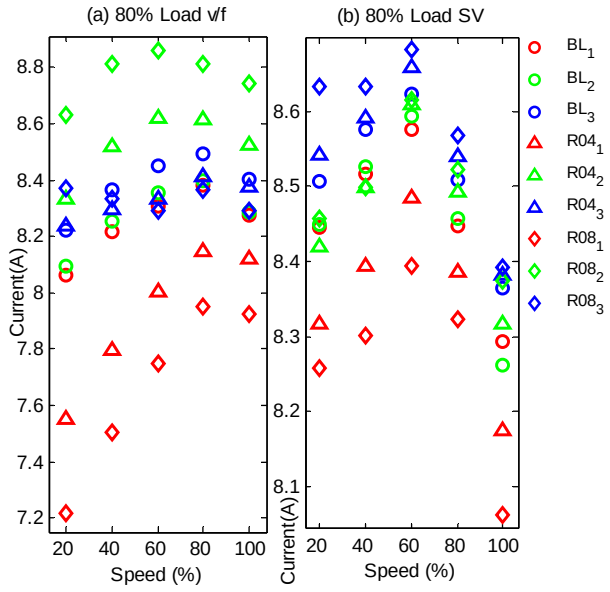

Figure 16. Plot of current for each phase at variable speed condition with 80% load setpoint for both drive modes. (a) *v/f* Mode (b) SV mode.

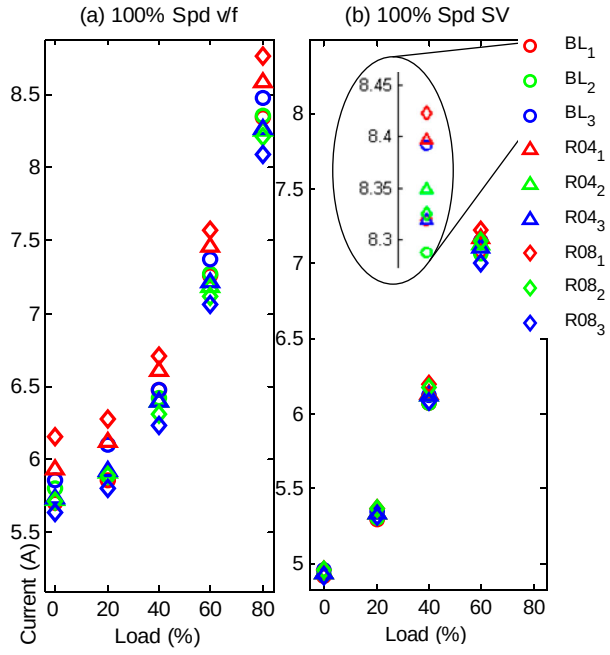

Figure 17. Plot of current for each phase at variable load condition with 100% speed setpoint. (a) *v/f* Mode (b) SV mode.

in SV mode, it can be seen that the imbalanced phase current separates from the healthy phase current but to a lesser extent than in *v/f* mode.

It is also notable from Figures 15–17 that the motor current and voltages are reduced under lighter motor loads in SV mode compared to *v/f* mode. as the drive makes more efficient use of motor electromagnetic torque at lighter loads.

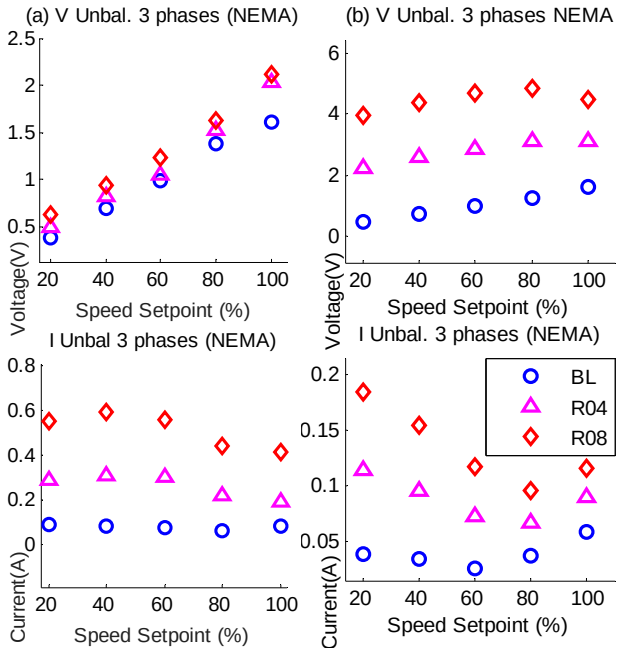

Figure 18. Voltage and current imbalances under NEMA definitions for variable speed. (a) *v/f* (b) SV.

BL_x: Baseline (Healthy Motor)
$R04_x$: Stator Resistance imbalance of 0.4 Ω;
$R08_x$: Stator Resistance imbalance of 0.8 Ω.
Ph1: Phase 1

where subscript $x = 1$ to 3 for each motor phase.

4.4. Motor current and voltage asymmetry

Figure 18 indicates the results of calculating motor voltage and current imbalances for the 80% load, variable speed test. This method makes comparing the voltage differences between healthy and faulty modes more straightforward than by comparing individual phases. The calculation method is in accordance with the NEMA definition. This defines a calculation for the Line Voltage Unbalance Rate (LVUR) as follows:

Suppose the average line voltage is calculated as

$$U_{\text{avg}} = \frac{U_{ab} + U_{bc} + U_{ca}}{3} \tag{14}$$

where U_{ab}, U_{bc} and U_{ca} represent the voltage between phases *a-b*, *b-c* and *c-a* respectively. If U_{avg} is the average line voltage and U_{ab} represents the phase with maximum voltage deviation, then the %LVUR is calculated as (Pillay & Manyage, 2001):

$$\%\text{LVUR} = \frac{U_{ab} - U_{\text{avg}}}{U_{\text{avg}}} \cdot 100 \tag{15}$$

However, in the MATLAB calculations for Figure 18, the actual voltage difference value is calculated in voltage

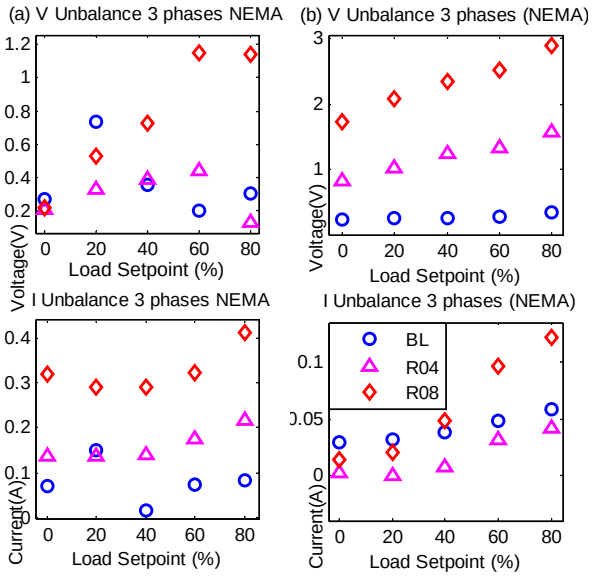

Figure 19. Voltage and current imbalances under NEMA definitions for variable load. (a) *v/f* (b) SV.

units rather than using a percentage value for clarity. The phase with maximum line voltage is calculated by the 'max' MATLAB function. The 'mean' function in MATLAB is used to calculate U_{avg} so:

$$\text{LVUR} = U_{ab} - U_{\text{avg}}. \tag{16}$$

BL: Healthy Motor (Baseline data);
R04: 0.4 Ω Fault resistance introduced in phase a
R08: 0.8 Ω Fault resistance introduced in phase a

The maximum voltage deviation when measured against the baseline is 3.697 V at 60% speed for the 0.8 Ω fault resistance in SV mode and 0.501 V at 80% speed in *v/f* mode. Maximum current deviation of 0.5071A is observed at 40% speed in *v/f* mode and 0.14387A in sensorless mode at 20% speed.

Figure 19 presents motor voltage and current imbalances for a variable load, constant 100% speed condition. The figures illustrate that for the voltage signals in SV mode (b), both imbalanced conditions of 0.4 Ω and 0.8 Ω can be identified. In *v/f* mode (a) the voltage results are inconclusive except for the 0.8 Ω resistance R08. The current readings show that there is a noticeable difference in current when the fault resistance is introduced in *v/f* mode (a). In SV mode (b) the current difference is only apparent at 60% load and above.

Maximum voltage deviation is 2.541 V at 80% load in SV operation and maximum current deviation is 0.08074A in *v/f* mode at 80% load.

BL: Healthy Motor (Baseline data);
R04: 0.4 Ω Fault resistance introduced in phase a
R08: 0.8 Ω Fault resistance introduced in phase a

4.5. Motor efficiency

This section contains the results of motor efficiency calculations based on three different methods:

- Shaft power estimation
- Electrical Input Power Estimation
- Efficiency based on the No Load Current Method.

These methods are described as follows:

To calculate shaft power, we firstly consider the instantaneous input power P of an AC motor, which is calculated as:

$$P = V_a I_{sa} + V_b I_{sb} + V_c I_{sc} \tag{17}$$

An average value of the instantaneous power for each load or speed setpoint sample is taken for these efficiency calculations. The shaft power is calculated as:

$$P_s = \left[\frac{1}{3}\left(\frac{\sigma(\overline{I_{sa}}) + \sigma(\overline{I_{sb}}) + \sigma(\overline{I_{sc}})}{I_{\text{rated}} \cdot P_{\text{rated}} \cdot (\omega_m/\omega_{\text{rated}})}\right)\right] \tag{18}$$

where $\overline{I_{sa}}$ represents the complete data set of current samples for phase current a taken at each load/speed point. ω_m represents the mechanical output speed in revolutions per second, ω_{rated} the motor rated speed, I_{rated} the motor rated current and P_{rated} the motor rated power.

The electrical input power calculation is based on the mean value of all the measured current and voltage signal samples:

$$P_i = \overline{(V_a I_{sa} + V_b I_{sb} + V_c I_{sc})} \tag{19}$$

The efficiency by current method uses the standard deviation of all data points for i_a, i_b, i_c with filter windows applied to calculate a single current value I_{abc} at each data sample set $\overline{I_{sa}}$ for each phase current *a, b, c*.

$$I_{abc} = \frac{1}{3}\sigma(\overline{I_{sa}}) + \sigma(\overline{I_{sb}}) + \sigma(\overline{I_{sc}}) \tag{20}$$

Based on the nameplate motor power rating, P_r a theoretical power output P_o is calculated based on the actual measured motor speed.

From these results, the efficiency η_I is calculated as follows:

$$\eta_I = \left[\left(\frac{2 \cdot (I_{abc} - I_m)}{2 \cdot I_{sr} - I_m}\right) \cdot \frac{P_r}{P_o}\right] \tag{21}$$

Where I_m is the magnetizing current, I_{sr} is the stator rated current.

Figure 20 indicates the result of these calculations. Motor shaft power is marginally increased under SV control, indicating better use of motor torque-producing

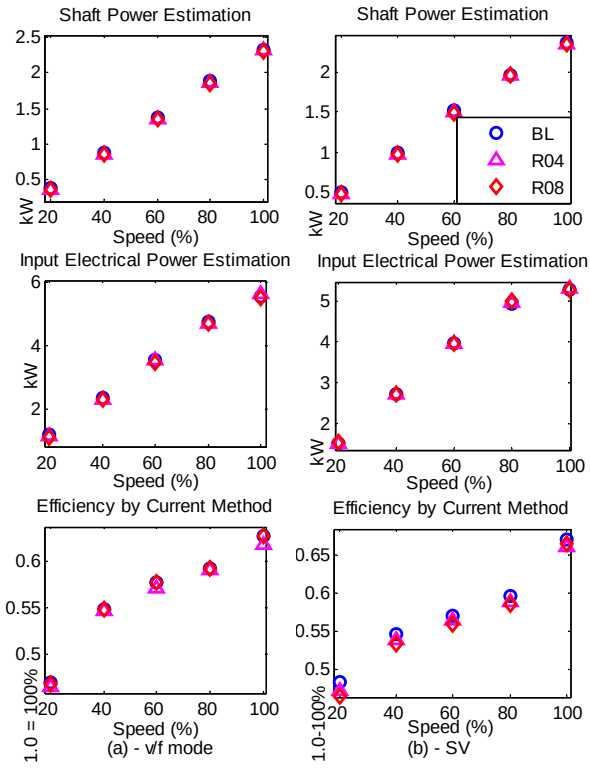

Figure 20. Plot of power estimation and efficiency using different techniques 80% load, variable speed; (a) *v/f* (b) SV.

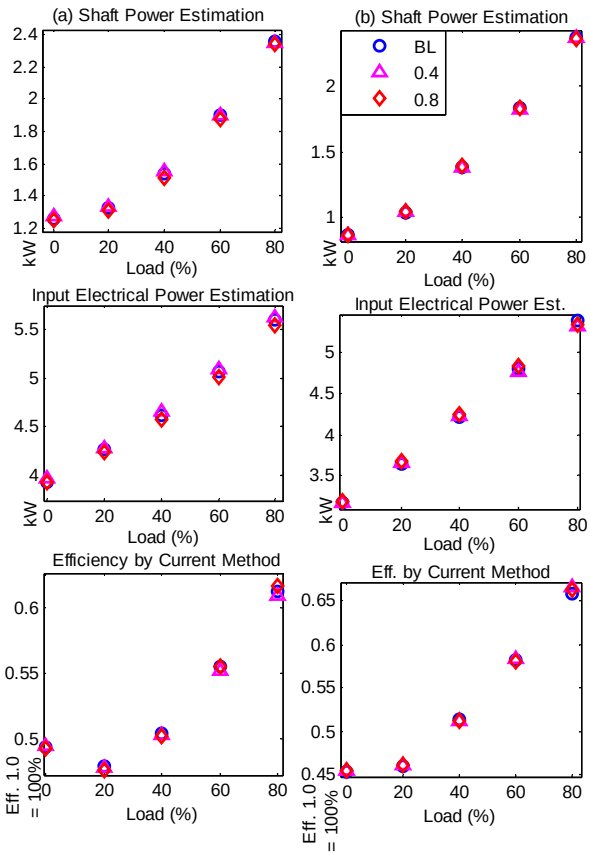

Figure 21. Plot of power estimation and efficiency using different techniques at a constant speed; (a) *v/f* (b) SV.

current due to the SV control algorithm. Calculations for electrical input power estimation show that effective input power is reduced under SV mode. The efficiency by current method calculations indicate that efficiency is increased with SV drive operation.

BL: Healthy Motor (Baseline data);
R04: 0.4 Ω Fault resistance introduced in phase a
R08: 0.8 Ω Fault resistance introduced in phase a

When the plots were examined in closer detail, it was not possible to clearly distinguish the healthy motor results from the results with imbalanced fault introduced.

Figure 21 represents the same calculation methods but for variable load conditions.

BL: Healthy Motor (Baseline data);
R04: 0.4 Ω Fault resistance introduced in phase a
R08: 0.8 Ω Fault resistance introduced in phase a

Under variable load operating conditions, it is shown that the shaft estimated power and motor input power is reduced for SV mode operation. However, the efficiency calculations show that under SV operation, efficiency is increased from the results under *v/f* mode.

For the purposes of detecting motor imbalance faults from all three calculation methods for *v/f* (a) and SV (b), the results are inconclusive as there is no clear difference between the healthy motor and one with an imbalanced fault introduced.

4.6. Motor efficiency by air gap torque method

This section presents the efficiency, η calculations based on the air gap torque method. The air gap torque T_{ag} is calculated after subtracting the stator resistance R_s, core and stator stray losses.

The following voltage equations apply for all stator windings where R_s is the stator (phase) resistance

$$v_{a,b,c} = \frac{\mathrm{d}\psi_{a,b,c}}{\mathrm{d}t} + R_S \cdot i_{a,b,c} \tag{22}$$

The air gap torque T_{ag} calculation used is given as (Lu, Habetler, & Harley, 2008):

$$T_{ag} = \frac{\sqrt{3}p}{6}\left\{(i_a - i_b) \bullet \int [v_{ca} + R_s(2i_a + i_b)]\,\mathrm{d}t + (2i_a + i_b) \bullet \int [v_{ab} - R_s(i_a - i_b)]\,\mathrm{d}t\right\} \tag{23}$$

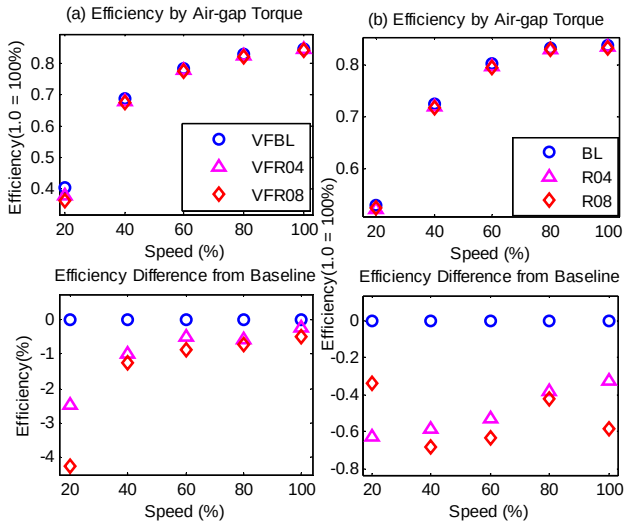

Figure 22. Motor efficiency calculations using air gap torque method at constant speed (a) *v/f* Mode (b) Sensorless.

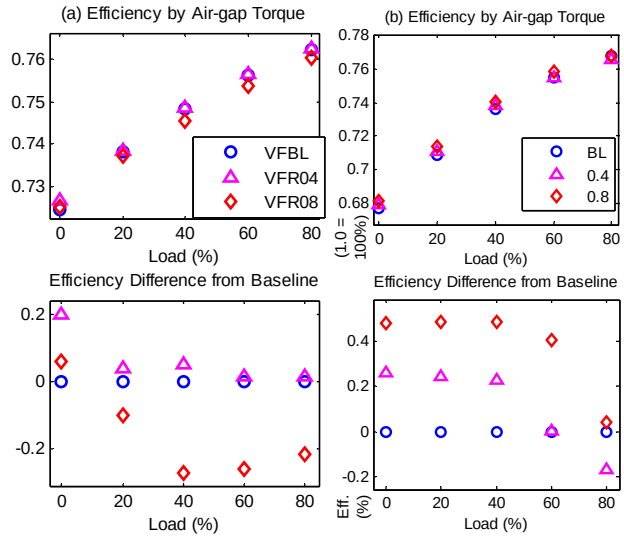

Figure 23. Motor efficiency calculations using air gap torque method at constant load (a) *v/f* Mode (b) Sensorless.

where v_{ca} and v_{ab} are the stator line voltages, i_a and i_b the stator currents. The integrals in this equation represent the corresponding flux linkages.

The efficiency calculation is expressed as

$$\eta = \frac{T_{sh} \cdot \omega_r}{P_{in}} = \frac{T_{ag} \cdot \omega_r - W_{fw} - W_{LLr}}{P_{\text{input}}} \qquad (24)$$

where T_{sh} is the torque at the motor shaft, W_{fw} is the friction and windage loss and W_{LLr} the rotor stray losses.

The Efficiency Difference from Baseline plots use the motor baseline efficiency measurements as the reference point for the plot. From this reference, any changes in efficiency due to the imbalance can be easier to observe.

BL: Healthy Motor (Baseline data);
R04: 0.4 Ω Fault resistance introduced in phase a
R08: 0.8 Ω Fault resistance introduced in phase a

From Figure 22, the motor running in SV mode (b) operates at decreased efficiency level of between 0.3% and 0.6% when motor imbalance faults are introduced. At 20% speed, the v/f mode drive is running 4% less efficient with the 0.8 Ω resistance increase. At 20% speed, the SV drive runs 0.4% less efficient. With increasing speeds in v/f mode, the efficiency reduction due to imbalance is smaller. In SV mode, the efficiency decrease remains relatively constant throughout the speed range.

BL: Healthy Motor (Baseline data);
R04: 0.4 Ω Fault resistance introduced in phase a
R08: 0.8 Ω Fault resistance introduced in phase a

Figure 23 indicates the same efficiency calculations for the constant speed variable load tests. In *v/f* mode (a), efficiency by air gap torque calculations only indicate a reduced efficiency in the motor with an imbalanced stator winding of 0.8 Ω. At 0% load setpoint, the efficiency calculation indicates an increase at 0.8 Ω imbalance. With a 0.4 Ω resistance imbalance the efficiency difference calculated is negligible. In sensorless vector control modes, the efficiency actually shows an increase in efficiency when the fault resistances are introduced but the difference from baseline can be observed. It is possible that the motor state model is disturbed by the introduction of fault resistances and operates more effectively but more information on the motor model is required to provide greater insight into the results.

4.7. Motor power factor – variable speed

Figure 24 shows the result of instantaneous power factor plots at each of the motor speeds and fault conditions. It can be observed that under the normal operating conditions, the motor power factor improves in line with the expected power factor curve given in Figure 5. An improvement in power factor is gained by the drive system operating in (b) sensorless vector control mode compared to a drive operating in (a) v/f mode. This is due to the drive constantly adjusting the torque '*q*' angle of the current component to maintain maximum torque producing current which improves the power factor. However, there is a marked reduction in power factor at full speed on the sensorless vector control plots.

BL: Healthy Motor (Baseline data);
R04: 0.4 Ω Fault resistance introduced in phase a
R08: 0.8 Ω Fault resistance introduced in phase a

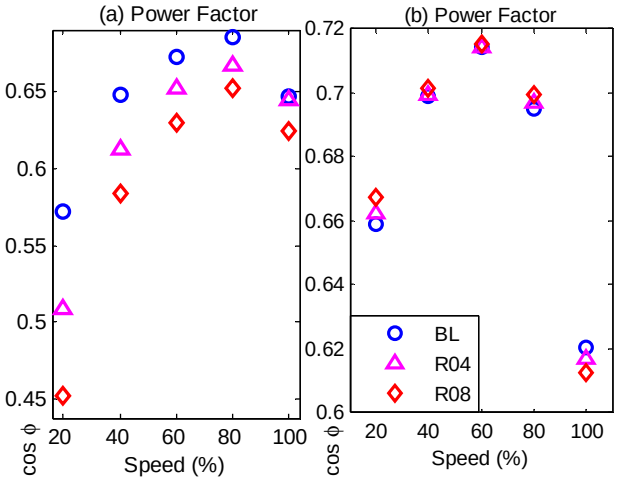

Figure 24. Motor power factor curves for a constant load with variable speed (a) *v/f* (b) SV.

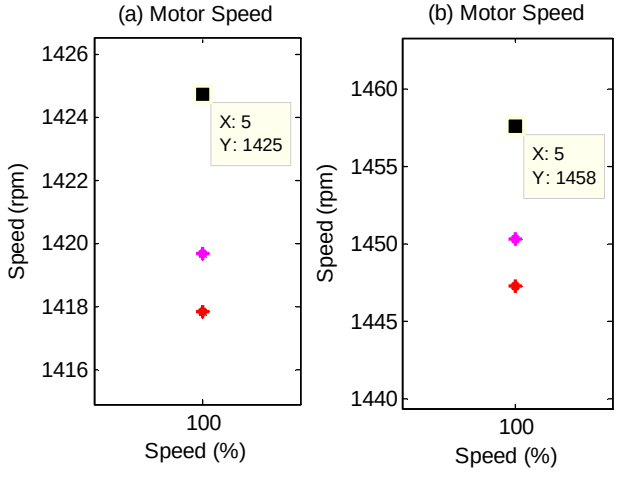

Figure 25. Motor actual measured speed from shaft-mounted encoder at 100% drive speed setpoint (a) *v/f* (b) SV.

This can be explained by the motor speed under sensorless drive control being driven beyond the maximum rated motor speed of 1420 RPM as can be observed in Figure 25.

Once the motor is speed is increased above the rated base speed then motor power factor is significantly reduced as observed in Figure 24 from 80% to 100% speed setpoint. The power factor is reduced from 0.7 to 0.62 between these two setpoints. The curve can be compared to that presented in Figure 5. The inverter drive settings for the motor were correct and these are given in Figure 26 so it can be concluded that there is an error with the drive internal motor speed observer.

This observer error causes the drive to estimate the motor speed to be lower than the actual speed. The drive now increases the output voltage and frequency to speed the motor up beyond the rated speed of 1420RPM. The

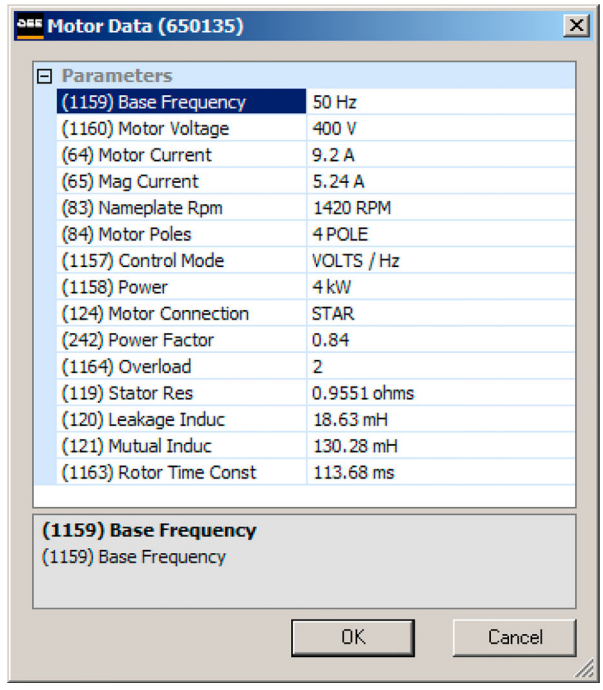

Figure 26. Motor settings in AC drive.

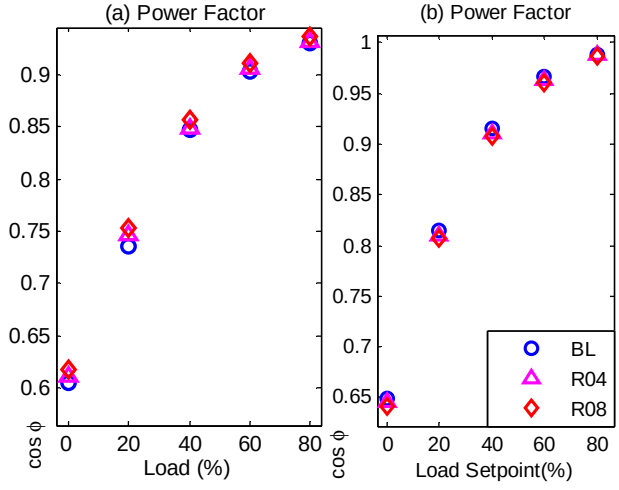

Figure 27. Motor power factor curves for drive modes (a) *v/f* (b) SV.

actual error was confirmed by the drive speed traces which for both v/f and SV modes indicated the drive estimated motor feedback speed to be 100%. The drive is calibrated so that 1420RPM = 100% speed for both v/f and SV modes. The drive speed observer error is for SV mode is 2.6% with the motor running at 1458RPM as measured in the tests. Traces taken from the drive diagnostics tools are included in appendix of this paper.

Figure 27 presents the power factor calculations for 100% speed, variable load conditions. There is no noticeable improvement in the motor power factor between

healthy and faulty conditions in either v/f SV drive modes.

BL: Healthy Motor (Baseline data);
R04: 0.4 Ω Fault resistance introduced in phase a
R08: 0.8 Ω Fault resistance introduced in phase a

5. Conclusions

This paper has demonstrated that it is possible to use time-domain motor current and voltage signals output from a PWM converter to differentiate between a healthy motor and a motor developing a graduated imbalanced fault on one stator winding. A variety of different calculations have to be used to provide a sufficient level of information on which to make a decision on which motor is healthy and which is faulty. This is also true when trying to determine the phase at fault.

The results show that the NEMA method of calculating imbalanced current and voltages is most effective at determining the motor with an imbalanced fault condition (Figures 18 and 19). An advantage of the NEMA method is that the reference data set could be sampled with the motor in service and under a range of load conditions. This method consistently indicated an increase in imbalance for current and voltage for variable load conditions as well as variable speed.

Efficiency calculations (Figures 22 and 23) detailing reductions in efficiency from the baseline data were only proved accurate for AV modes (b). For drives operating in this mode, a reduction in efficiency of 0.3% and 0.6% was observed in Figure 22(b). This reduction would not be cause for concern under general operation and may be difficult to detect in real-world conditions but would provide a useful early indicator for early intervention investigations. If it is proven that the techniques are sensitive enough to detect this reduction in efficiency reliably and repeatedly, then intervention field tests could be scheduled for efficiency losses greater than 1%.

Power factor measurement techniques on the signals (Figures 24 and 27) obtained from the drive under variable speed conditions at a constant load indicate that power factor is improved when the drive is operated in SV mode compared with v/f. Given the choice of drive operating modes at installation, it is clearly advisable to operate a VSD drive in SV mode to improve efficiency and power factor. However, the test results also indicate that although the drive calibration parameters were set to a maximum motor speed of 1420RPM, errors can occur in drive speed observer models even on autotuned motors. In these tests, it was shown that the motor in was driven beyond its most efficient operating speed of 1420RPM by the drive. It is unlikely that the end user of the equipment would measure the actual mechanical speed by means of a tacho once running. This means that the efficiency of the installation is compromised from the outset. The methods described in this paper could be used in the field to provide a final check of system operating conditions before the equipment is put into service. This would at least indicate to an engineer any abnormalities in operation prior to signing off the installation and commissioning as complete.

This paper also indicates that for motors operating at less than full load, choosing a SV VSD drive may make more economic sense when total running costs (purchase cost + energy consumption) are considered. The initial purchase cost may be higher but because of the reduced energy consumption of the motor at lighter loads in SV mode, the payback from energy savings could quickly be realized to justify the higher initial outlay.

The efficiency calculations are less conclusive for reduced motor loads but it is well known that motors are less efficient when operating under reduced load conditions. As a rule, motors should always be sized to operate towards their full load rating to maximize efficiency of the installation.

Future work is planned on the model simulation of this system along with fault condition estimators.

Disclosure statement

No potential conflict of interest was reported by the authors.

References

Akar, M., & Gercekcioglu, H. S. (2017). Instantaneous power factor signature analysis for efficient fault diagnosis in inverter fed three phased induction motors. *Energy Weekly News*. ISSN: 1945-6980. June 2017. p. 510. Retrieved from https://search.proquest.com/docview/1910226320?accountid=11526

Arabacı, H., Bilgin, O., & Ürkmez, A. (2011). *Rotor bar fault diagnosis by using power factor*. Proceedings of the world congress on engineering 2011 Vol II WCE 2011, July 6–8, 2011, London, UK, pp. 981–984. Retrieved from http://www.iaeng.org/publication/WCE2011/WCE2011_pp981-984.pdf

Bonnett, A. H., & Soukup, G. C. (1992). Cause and analysis of stator and rotor failures in three phase squirrel-cage induction motors. *IEEE Transactions On Industry Applications*, *28*(4), 921–937.

BS EN 60034-2-1:2014 Rotating electrical machines Part 2-1: Standard methods for determining losses and efficiency from tests (excluding machines for traction vehicles). ICS 29.160.30. ISBN 978 0 580 56364 5. pp. 21, 22.

Crowder, R. (2006). *Electric drives and electromechanical systems 1st edition*; Paperback ISBN: 9780750667401; eBook ISBN: 9780080492643; Imprint: Newnes; Published Date: 25th January 2006; p. 196.

DD CLC/TS 60034-25:2008 Rotating electrical machines. Guidance for the design and performance of a.c. motors specifically

designed for converter supply. ICS 29.160.30, ISBN 978 0 580 56364 5. pp. 19-20, 63

de Souza-Ribeiro, L. A., Jacobina, C. B., Nogueira Lima, A. M., Cunha Oliveira A. (1997). Parameter sensitivity of MRAC models employed in IFO-controlled AC motor drive. *IEEE Transactions on Industrial Electronics*, *44*(4), 536–545. doi:10.1109/41.605631

Drif, M., & Marques Cardoso, A. J. *The instantaneous power factor approach for rotor cage faults diagnosis in three-phase induction motors*. International symposium on power electronics, electrical drives, automation and motion. P - 3030-290 Coimbra, Portugal, pp. 173–178. doi:10.1109/SPEEDHAM.2008.4581170

Efficiency classes for IEC line motors. Retrieved from http://w3.siemens.com/drives/global/en/motor/low-voltage-motor/efficiency-standards/pages/line-motors.aspx

Hou, X., Gu, Z., Gao, X., Feng, S., & Li, Y. (2008, July). *Analysis of efficiency and power factor of reciprocating compressor unit under variable frequency and variable-conditions*. International compressor engineering conference, pp. 1222, 1–7. Retrieved from http://docs.lib.purdue.edu/icec/1878

Ibrahim, A., Badaoui, M. E., Guillet, F., & Bonnardot, F. (2008). A New bearing fault detection method in induction machines based on instantaneous power factor. *IEEE Transactions on Industrial Electronics*, *55*(12), 4252–4259. doi:10.1109/TIE.2008.2003211

Karmakar, S., Chattopadhyay, S., Mitra, M., & Sengupta., S. (2016). *Induction motor fault diagnosis, power systems*. doi:10.1007/978-981-10-0624-1_2 © Springer Science + Business Media Singapore. chap. 2, p. 20. Retrieved from https://link.springer.com/chapter/10.1007%2F978-981-10-0624-1_2

Kirschen, D. S., Novotny, D. W., & Suwanwisoot, W. (1984). Minimizing induction motor losses by excitation control in variable frequency drives. *IEEE Transactions On Industry Applications*, *IA-20*(5), 1244–1250.

Lee, S. B., Yang, J., Hong, J., Yoo, J-Y., Kim, B., Lee, K., . . . Nandi, S. (2011). A new strategy for condition monitoring of adjustable speed induction machine drive systems. *IEEE Transactions On Power Electronics*, *26*(2), 389–398. doi:10.1109/TPEL.2010.2062200

Li, Y., Liu, M., Lau, J., & Zhang, B. (2015). A novel method to determine the motor efficiency under variable speed operations and partial load conditions. *Applied Energy*, *144*, 234–240. doi:10.1016/j.apenergy.2015.01.064

Lu, B., Habetler, T. G., & Harley, R. G. (2008). A nonintrusive and in-service motor-efficiency estimation method using air-gap torque with considerations of condition monitoring. *IEEE Transactions On Industry Applications*, *44*(6), 1666–1674. doi:10.1109/TIA.2008.2006297

McCoy, G. A., & Douglass, J. G. (2000). *Energy management for motor-driven systems*. Washington State University. Revision 2 March 2000. pp. 3-4, 5-1. Retrieved from https://energy.gov/sites/prod/files/2014/04/f15/NN0116.pdf

Meza, M. (2014). *Industrial LV motors & drives: A global market update*. Motors & Drive Systems 2014, Advancements in Motion Control and Power Electronic Technology, January 29–30, Orlando, USA, p. 6. Retrieved from www.e-driveonline.com/conferences/wp-content/uploads/2014/01/IHSMMeza.pdf

Mirabbasi, D., Seifossadat, G., & Heidari, M. (2009). *Effect of unbalanced voltage on operation of induction motors and its detection*. International conference on electrical and electronics engineering ELECO 2009; pp. I-189 - I-192. pp. I-189. doi:10.1109/ELECO.2009.5355288

Mouli Chandra, B., & Tara Kalyani, S. (2012). *Online estimation of stator resistance in vector control of induction motor drive*. IEEE fifth power India conference. doi:10.1109/PowerI.2012.6479478

Office of Energy Efficiency and Renewable Energy U.S. Department of Energy; United States Industrial Electric Motor Systems Market Opportunities Table E-1 p.9. Retrieved from https://www.energy.gov/sites/prod/files/2014/04/f15/mtrmkt.pdf

Pillay, P., & Manyage, M. (2001). Definitions of voltage unbalance. *IEEE Power Engineering Review*, *21*(5), 50–51. p. 51. doi:10.1109/39.920965.

Rao, N., & Chamund, D. (2014). *Calculating power losses in an IGBT module*. Application Note AN6156-1, September 2014 LN31943. p. 12. Retrieved from https://www.dynexsemi.com/assets/downloads/DNX_AN6156.pdf

Rasool, S., & Ebrahimi, M. (2011). Detection of stator winding faults in induction motors using three-phase current monitoring. *ISA Transactions*, *50*(1), 14–20. doi:10.1016/j.isatra.2010.10.008

Salomon, C. P., Sant'Ana, W. C., Borges da Silva, L. E., Lambert-Torres, G., E. L. Bonaldi, L. E. L. de Oliveira, & J. G. Borges da Silva. (2015). Induction motor efficiency evaluation using a new concept of stator resistance. *IEEE Transactions On Instrumentation And Measurement*, *64*(11), 2908–2917. doi:10.1109/TIM.2015.2437632

Shnibha, R. A., & Albarabar, A. S. (2012). *Smart technique for induction motors diagnosis by monitoring the power factor using only the measured current*. 25th international congress on condition monitoring and diagnostic engineering, journal of physics, conference series 364 012062. Retrieved from http://iopscience.iop.org/article/10.1088/1742-6596/364/1/012062/pdf

Siemens Energy Efficient Drives – Answers for Industry. p. 4. Retrieved from https://w3.siemens.com/mcms/water-industry/en/Documents/Energy-Efficient_Drives.pdf

Siemens Sinamics S120 Drive Functions Function Manual. 01/2013 (FH1), 01/2013 6SL3097-4AB00-0BP3. Copyright © Siemens AG 2004–2013. p. 212. Retrieved from https://support.industry.siemens.com/cs/attachments/49084671/FH1_012011_eng_en-US.pdf

Trzynadlowski, A. M. (2001). Control of induction motors; Copyright © 2001 by Academic Press; ISBN: 0-12-701510-8; p. 34.

Zaky, M. S. (2012). Stability analysis of speed and stator resistance estimators for sensorless induction motor drives. *IEEE Transactions On Industrial Electronics*, *59*(2), 858–870. doi:10.1109/TIE.2011.2161658

Zhang, J., Zhao, J., Zhou, D., & Huang, C. (2014). High-performance fault diagnosis in PWM voltage-source inverters for vector-controlled induction motor drives. *IEEE Transactions On Power Electronics*, *29*(11), 6087–6099. doi:10.1109/TPEL.2014.2301167

Appendix

Speed and current traces from drive data logging software tools.

Figure 28 represents (a) Open-loop or v/f mode. Figure 28 represents (b) Sensorless Vector SV mode. Traces are shown for the drive operating in a constant-load 80% setpoint, variable speed condition. These traces are included to support the evidence obtained of the sensorless controller estimating the rotor speed incorrectly.

The drive was calibrated for a base motor speed of 1420 RPM which equates to 100% speed feedback in the diagram below.

In *v/f* mode, the motor speed estimated by the drive is 100% of motor base speed (1420RPM) and the actual measured mechanical speed was 1425RPM. This represents a difference of 5 RPM, or 0.35% speed error.

Red – Motor Speed; Blue – Motor Torque; *Y*-axis %, *x*-axis Time (s).

Figure 29 presents the same plot but for SV mode. Here, the motor speed estimated by the drive is 100% of motor base speed (1420RPM) but the actual measured mechanical speed was 1458RPM. This represents a difference of 38 RPM, or 2.67% speed error.

Red – Motor Speed; Blue – Motor Torque; *Y*-axis %, *x*-axis Time (s).

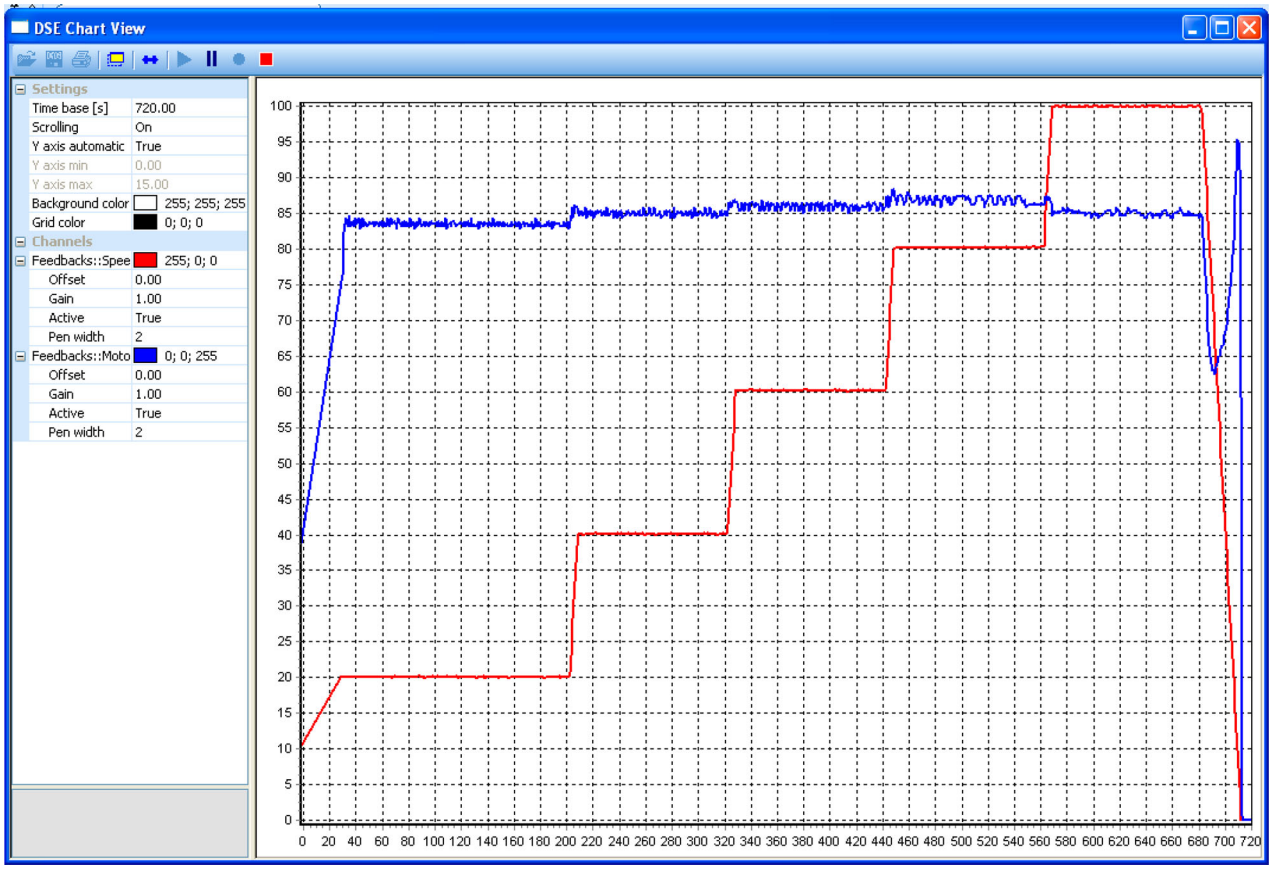

Figure 28. Drive running in *v/f* mode at 80% load setpoint, variable speed with no fault resistance introduced. Note that the estimated motor speed by the drive was 100% whilst the motor actual speed measured was 1425 RPM.

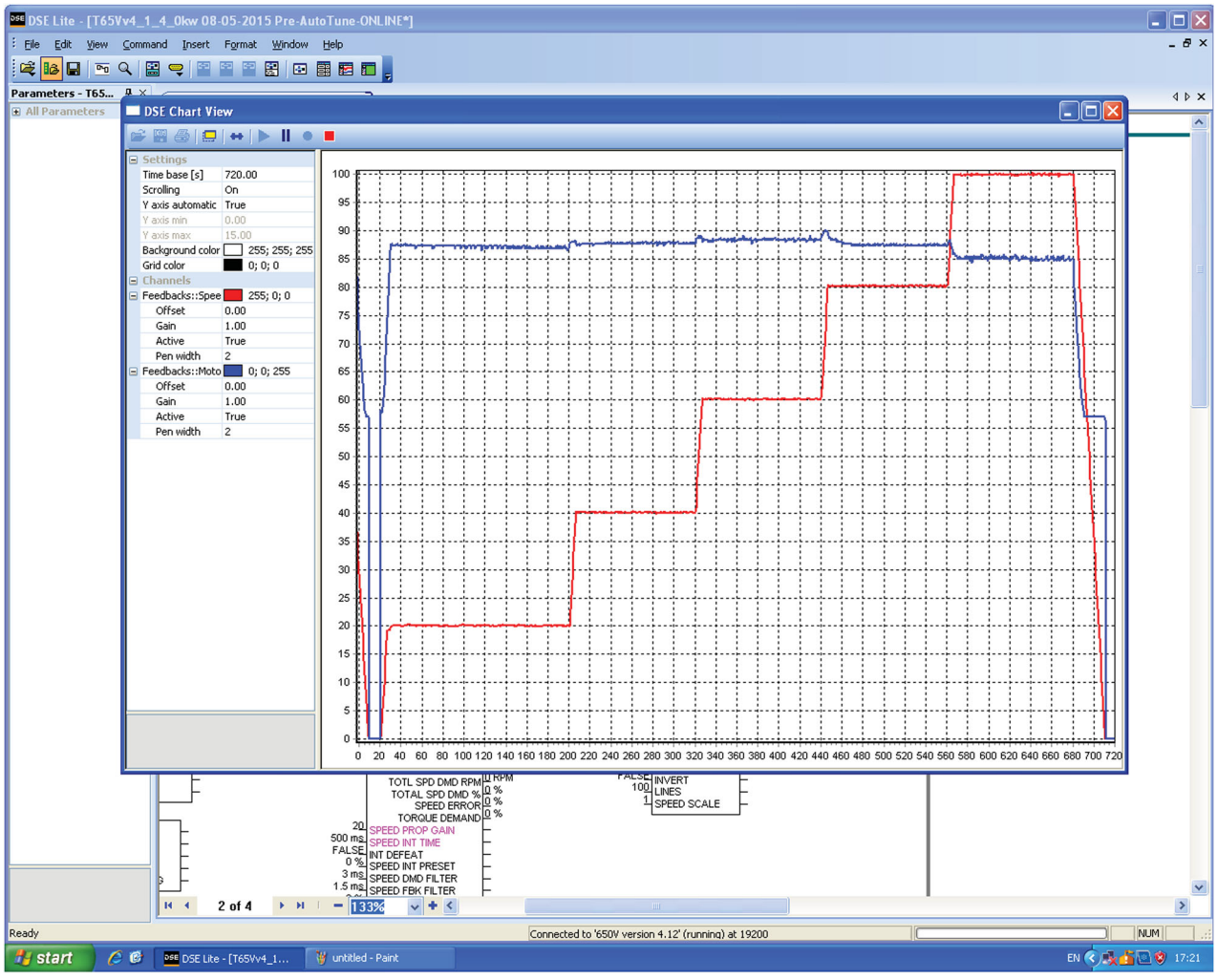

Figure 29. Drive running in sensorless vector mode at 80% load setpoint 100% speed with no fault resistance introduced. Note that the estimated motor speed of the drive was 100% whist the motor actual speed measured was 1458 RPM.